Manufacturing Rev. **9**, 25 (2022)

https://doi.org/10.1051/mfreview/2022023

Manufacturing Review
Available online at:
https://mfr.edp-open.org

RESEARCH ARTICLE OPEN ACCESS

Study on tensile and fatigue failure in the low-hardness zone of AA2519-T62 FSW joint

Robert Kosturek*, Tomasz Ślęzak, Janusz Torzewski, Marcin Wachowski, and Lucjan Śnieżek

Military University of Technology, Faculty of Mechanical Engineering, 2 gen. S. Kaliskiego str., 00–908 Warsaw, Poland

Received: 6 May 2022 / Accepted: 2 August 2022

Abstract. The aim of this research was to investigate the basic performance and failure of AA2519-T62 friction stir welded joint in tensile test and in low cycle fatigue regime. It has been reported that at the retreating side, the layer of overgrowth grains undergoes deformation in the TMAZ and forms a characteristic large-grain band partly surrounding the SZ. The reported UTS is very high and it equals 405 MPa, what corresponds to 86.5% joint efficiency value. The failure occurred in the LHZ at the retreating side with the fracture mechanism characterized by simultaneously cracking in several parallel planes. The LCF behavior of the tested joint indicates three stages of fatigue life: a relatively long period of cyclic hardening (up to 500–1000 cycles), the longest period of cyclic stabilization, followed by cyclic softening until failure. The fatigue crack initiation takes place in the near-surface layer of overgrown grains and then propagates through the low-hardness zone.

Keywords: Aluminum / friction stir welding / microstructure / mechanical properties / low cycle fatigue / fracture

1 Introduction

Friction stir welding (FSW) is a very effective technique dedicated to joining light metals, predominantly aluminum alloys. Its increasing popularity in industry owes to high-quality joints and low energy consumption, compared to other, more commonly used, welding techniques [1]. Because of its solid-state nature, FSW significantly limits the risk of hot cracking, and the presence of pores and provides an ultra-fine grain microstructure of the stirred area, giving joints excellent mechanical properties [2–5]. As in every welding process, an unavoidable drop in mechanical properties has to be examined to predict the joint's behavior in load-carrying operation. When it comes to aluminum alloys, precipitation-hardened ones are of great engineering interest for their high specific strength, and often good ballistic properties, what makes them widely used materials in the military industry [6–9]. AA2519 is an excellent example of armor grade aluminum alloy of the 2XXX series (Al-Cu), which owes its superior mechanical properties to the precipitation hardening process, and it is used as a structural material in light military vehicles [10,11]. Furthermore, the modification of AA2519 alloy has been developed by the Institute of Non-Ferrous Metals, Light Metals Division in Skawina and it is characterized by a higher concentration of scandium and zirconium, providing grain refinement, increase in temperature of recrystallization, and inhibiting grain growth [12–14]. In FSW of a precipitation-hardened aluminum alloy, a relatively high reduction of mechanical properties is expected, predominantly due to an overaging of strengthening phases [8,15]. For this reason, a lot of effort is put into studies on FSW of 2XXX and 7XXX alloys in terms of welding parameters optimization [16–18] including also different cooling media [19] and joints post-processing [20–22].

Considering the structural integrity of these welded joints, the weakest point is often linked to the softest region, which is the low-hardness zone (LHZ) [1,19,23]. The zone is located at the boundary between the heat-affected zone (HAZ) and thermo-mechanically affected zone (TMAZ) with their size and properties depending on FSW process parameters [23,24]. It has been reported by many scientists that LHZ is responsible for decreasing fatigue properties of FSW joints, what is predominantly the effect of larger grain size and coarse precipitates resulting in easier crack initiation and propagation e.g. in AA2219-T6 joints [19]. On the other hand, some reports point out that rough friction stir welded surface is one of the main causes of the fatigue failure at the stir zone (SZ) of AA2219-T6 [25]. SZ is additionally characterized by a high fraction of high-angle grain boundaries where the cracks were easier to appear [25,26]. The other factor which influences the fatigue failure of considered joints is the morphology of second-phase inclusions (Al_2Cu precipitates) [19]. For these precipitates do undergo partial

* e-mail: robert.kosturek@wat.edu.pl

Table 1. Chemical composition and basic mechanical properties of AA2519 alloy.

Chemical composition (in weight percent)											
Fe	Si	Cu	Zn	Ti	Mn	Mg	Ni	Zr	Sc	V	Al
0.11	0.08	6.32	0.05	0.08	0.17	0.33	0.02	0.19	0.16	0.10	Base
Mechanical properties											
Yield Strength, $R_{0,2}$			Tensile Strength, R_m			Fracture Stress, R_u			Elongation, A		
312 MPa			469 MPa			434 MPa			19%		

Table 2. The dimensions of the used MX Triflute tool.

Shoulder profile	Spiral
Shoulder diameter	19 mm
Pin profile	Threaded and tapered with three spiral flutes
Pin length	4.8 mm
Pin diameter	6.5–8.7 mm

fragmentation (predominantly in the SZ) their distribution and size are different in various parts of an FSW joint. This phenomenon plays an important role considering the fact that large Al_2Cu precipitates (non-coherent in their nature) serve as stress risers affecting crack initiation and propagation [19,22]. Another complexity in describing crucial factors determining fatigue properties of FSW joints is the differences in mechanical properties of each zone. It has been established during mini-specimen tensile tests of 2219-T87 FSW joint, that tensile strength reaches its highest value for HAZ, and for SZ and TMAZ the obtained result is almost the same and it is about 12% lower than in the case of HAZ [26]. At the same time, the ductility behaves opposite, the highest value concerned SZ and TMAZ, and the HAZ is characterized by the lowest elongation to break [26]. Also, the differences in grainy microstructure, especially in severely deformed areas can strongly promote decohesion, often leading to failure in low-cycle fatigue regime at high total strain amplitudes [27,28].

In this paper, the main goal is to study selected factors promoting decohesion in the low hardness zone of AA2519-T62 FSW joint in tensile test and low cycle fatigue test (at total strain amplitude of $\varepsilon = 0.3\%$), including macro and microstructural analysis, microhardness distribution, and the observations of fracture surfaces.

2 Materials and methods

The workpiece to be welded was AA2519 extrusion with the chemical composition and basic mechanical properties given in Table 1.

The dimensions of extruded workpiece were equal to $80 \times 250 \times 5$ mm. Before the welding, the material has been subjected to the precipitation hardening process by two-step heat treatment: solution treatment (530 °C/2 h followed by cooling in cold water) and artificial aging (165 °C/10 h). The welding process has been performed on ESAB FSW Legio 4UT using the following welding parameters: 400 rpm tool rotation speed, 10 cm/min tool traverse velocity, MX Triflute as the tool, and 4.8 mm plunge depth. This type of tool consists of a tapered probe body and three equally spaced helical flutes [1]. The dimensions of the MX Triflute are given in Table 2.

The obtained welded joint (Fig. 1) has been taken under investigation in terms of macro and microstructure, tensile test, low cycle fatigue, and fracture surface observations.

After the welding samples have been cut in the direction perpendicular to the welding direction. The macrostructure analysis involved a digital light microscope Olympus LEXT OLS 4100. The used etchant was Keller's reagent consisting of 20 mL H_2O, 5 mL 63% HNO_3, 1 mL 40% HF, and one drop of 36% HCl. The analysis was also supported by Vickers microhardness distribution using 0.98 N load. The distribution of microhardness was obtained for the three different levels of the cross-section of the weld: top, middle, and bottom localized at 0.8, 2.5, and 4.4 mm from the face of the joint, respectively. The tensile test was carried out on INSTRON 8802 MTL supported by WaveMatrix software. The low-cycle fatigue testing was performed on Instron 8802 Servohydraulic Fatigue Testing System on the total strain amplitude of 0.3% with $R = 0.1$ strain ratio. The schemes of the samples are presented below (Fig. 2).

The samples have been slightly grounded in the weld face area to minimalize the influence of surface irregularities and roughness on the fatigue performance of the joint. The fracture surfaces of tensile and fatigue samples were analyzed on scanning electron microscope (SEM) Jeol JSM-6610.

3 Results and discussion

The observation of the weld face did not reveal any imperfection (Fig. 1). FSW causes changes in the surface geometry of welded workpieces, forming the typical "ringed" weld face (Figs. 1 and 3). These irregularities act like notches in a condition of cyclic loading and strongly promote a crack initiation.

Fig. 1. The image of the obtained FSW joint.

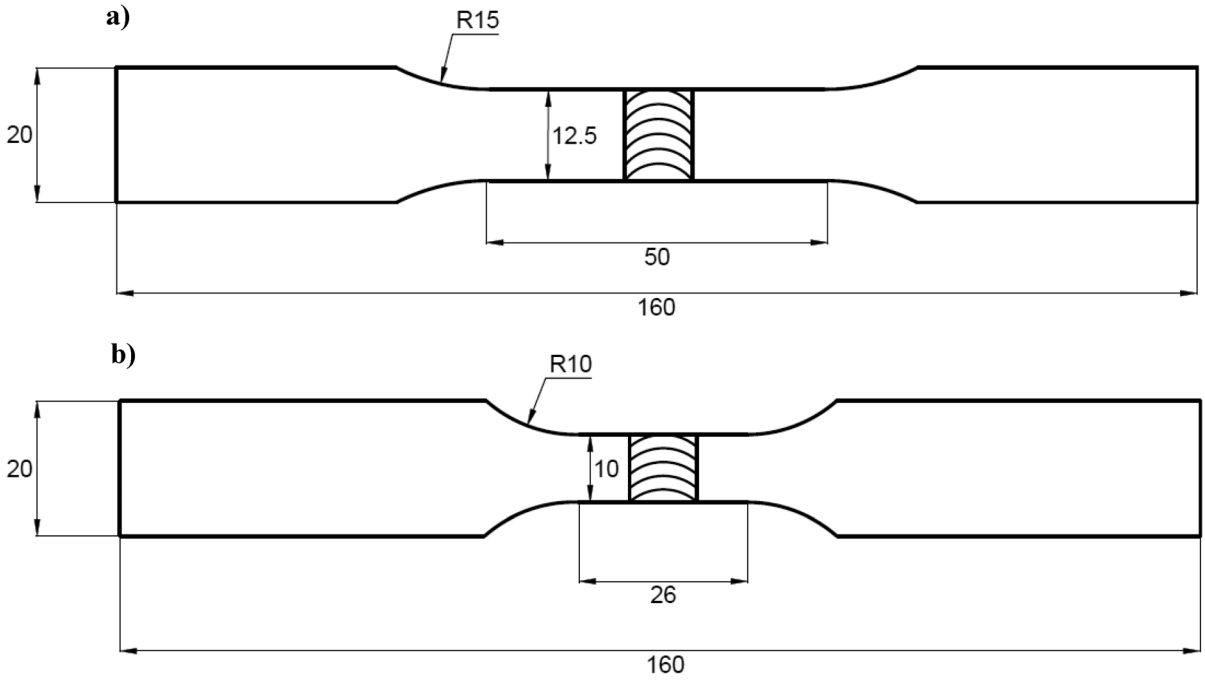

Fig. 2. The scheme of the sample for (a) tensile test, (b) low-cycle fatigue testing.

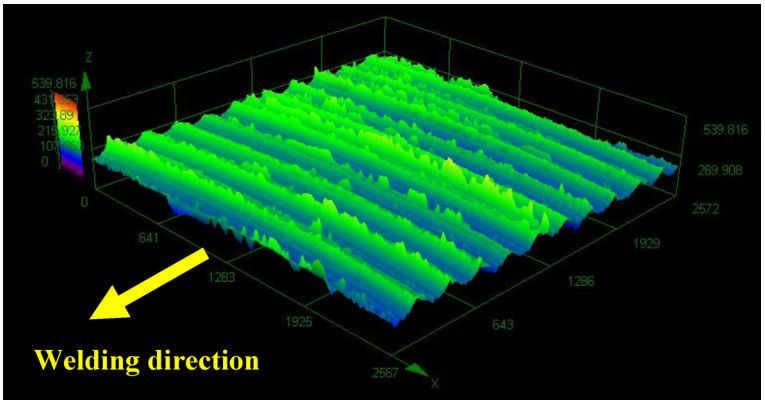

Fig. 3. The weld face surface geometry with marked welding direction.

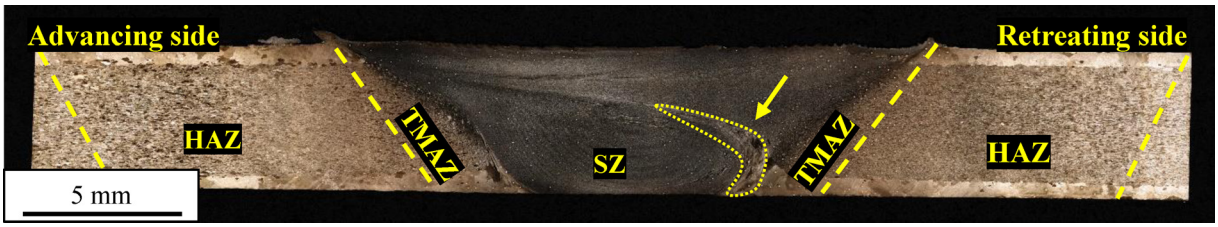

Fig. 4. The macrostructure of the FSW joint. Partly stirred large grains marked with yellow arrow.

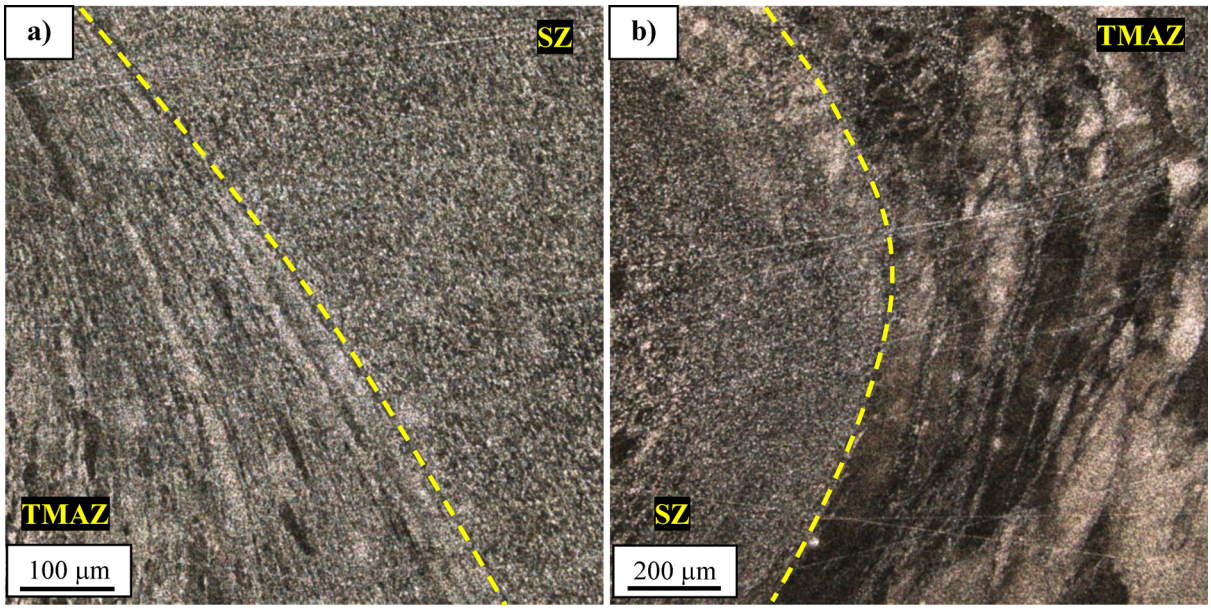

Fig. 5. The microstructure of FSW joint. (a) TMAZ/SZ interface at the advancing side. (b) TMAZ/SZ interface at the retreating side.

The macrostructure of the obtained joint is presented in Figure 4, with a distinguished advancing side (where the linear velocity vector of the rotating tool and the welding direction are one and the same) and retreating side (where the linear velocity vector of the rotating tool and the welding direction are opposite to each other).

The obtained joint is free of imperfections and has a very low reduction of the workpiece thickness in the weld zone (4.7 mm). The observations of the joint's macrostructure allow stating that the grainy microstructure in the stirred region did undergo severe refinement. A noteworthy aspect is the base material has some differences in grainy microstructure on its cross-section. At the top and bottom, the grains have a larger size, what is probably the effect of grain growth during solution treatment of the raw extrusion. These grains were partly stirred during the welding process, forming a characteristic tail trailing from the workpiece bottom through the SZ/TMAZ boundary (marked with the yellow arrow in Fig. 4). The selected images of the FSW joint microstructure are presented below (Figs. 5a,5b).

Typically for FSW joint, the welding process caused a significant refinement of grainy structure in the stir zone due to the dynamic recrystallization process. The stir zone's grainy microstructure is homogenous and is characterized by grain size of 10 µm. On both sides, the thermo-mechanically affected zone consists of deformed, elongated grains (Fig. 5a), although it can be observed that in the case of the retreating side the larger grains did not undergo such severe deformation and partly maintain their grain size forming a layer half surrounding the stir zone (Fig. 5b).

The obtained microhardness distribution on the joint's cross-section is presented on the graph (Fig. 6).

All three lines exhibit a similar shape, which corresponds to the typical "W"-shaped microhardness curve for friction stir welded precipitation-hardened aluminum alloys. Despite the affecting of high temperature in the stir zone region, the formation of fine-grained microstructure entails a relatively high value for a welded joint. Considering the stir zone, it can be seen that for the line closest to the weld's crown the microhardness value is about 115–120 HV0.1. Similar values are reported for the middle line, although the greater spread of results is noticeable. The microhardness value tends to decrease for the line localized at the joint's root, equal to about

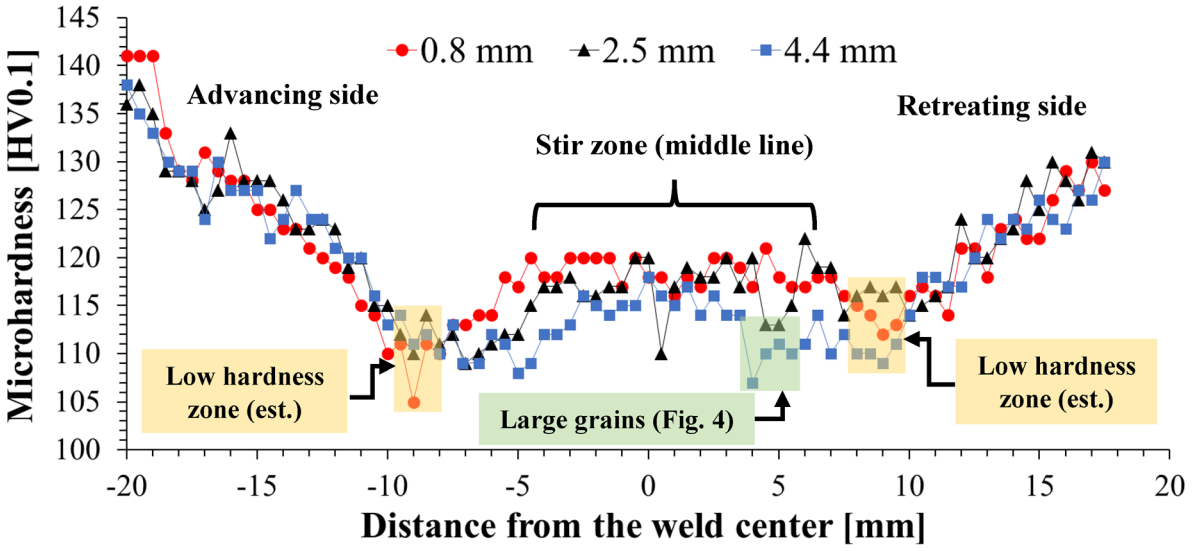

Fig. 6. The microhardness distribution of FSW joint.

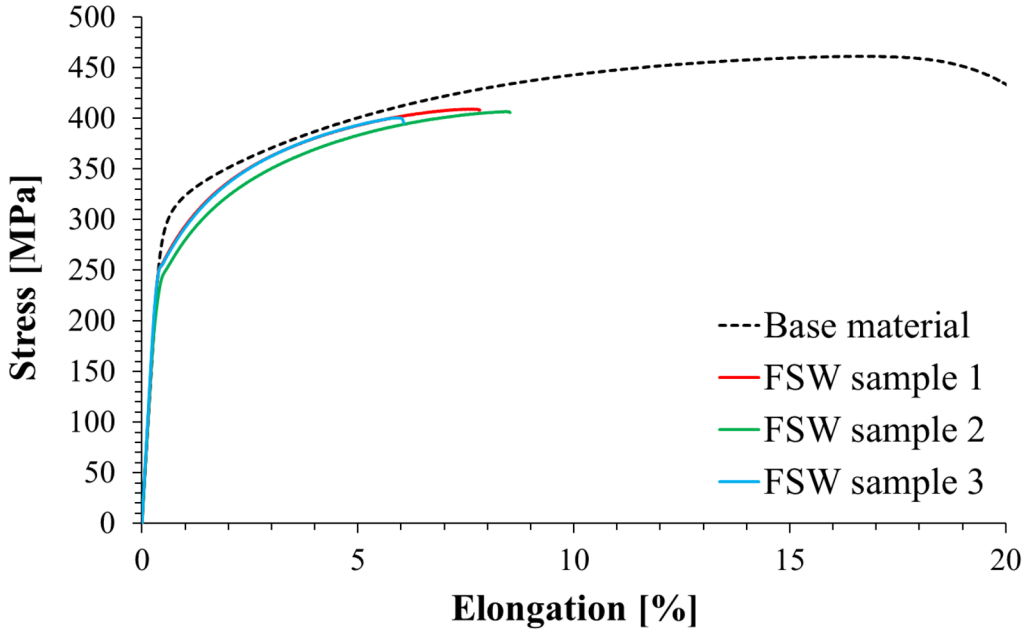

Fig. 7. Base material and FSW joints stress-strain curves from the tensile tests.

115 HV0.1. The low hardness zones have been identified at the distance of 8–10 mm (estimated 2 mm width) from the weld's center for each side. It is an estimation based on the average drop in microhardness for all three lines, but the exact location of this zone changes along with the sample's high due to uniform deformation and temperature distribution. The obtained localization of the low hardness zones is in line with the literature data [6,23]. It has been reported that in the case of the middle (2.5 mm) and bottom line (4.4 mm), the thermo-mechanically affected zone, closest to the stir zone, takes relatively low values of microhardness, which contain within the range of 107–113 HV0.1. This is probably the effect of the large grains, partly stirred into this area (Figs. 4 and 5b).

The obtained tensile curves for the investigated joints and for the base material are presented below (Fig. 7).

The produced joint is characterized by very high repeatability in terms of tensile testing, the average ultimate tensile strength is 405.6 ± 6.1 MPa, what corresponds to joint efficiency of $86.5 \pm 1.3\%$. At the same time, the elongation to break of the joint is relatively low with the reported value of $8.3 \pm 0.4\%$, allowing to state a 11% drop

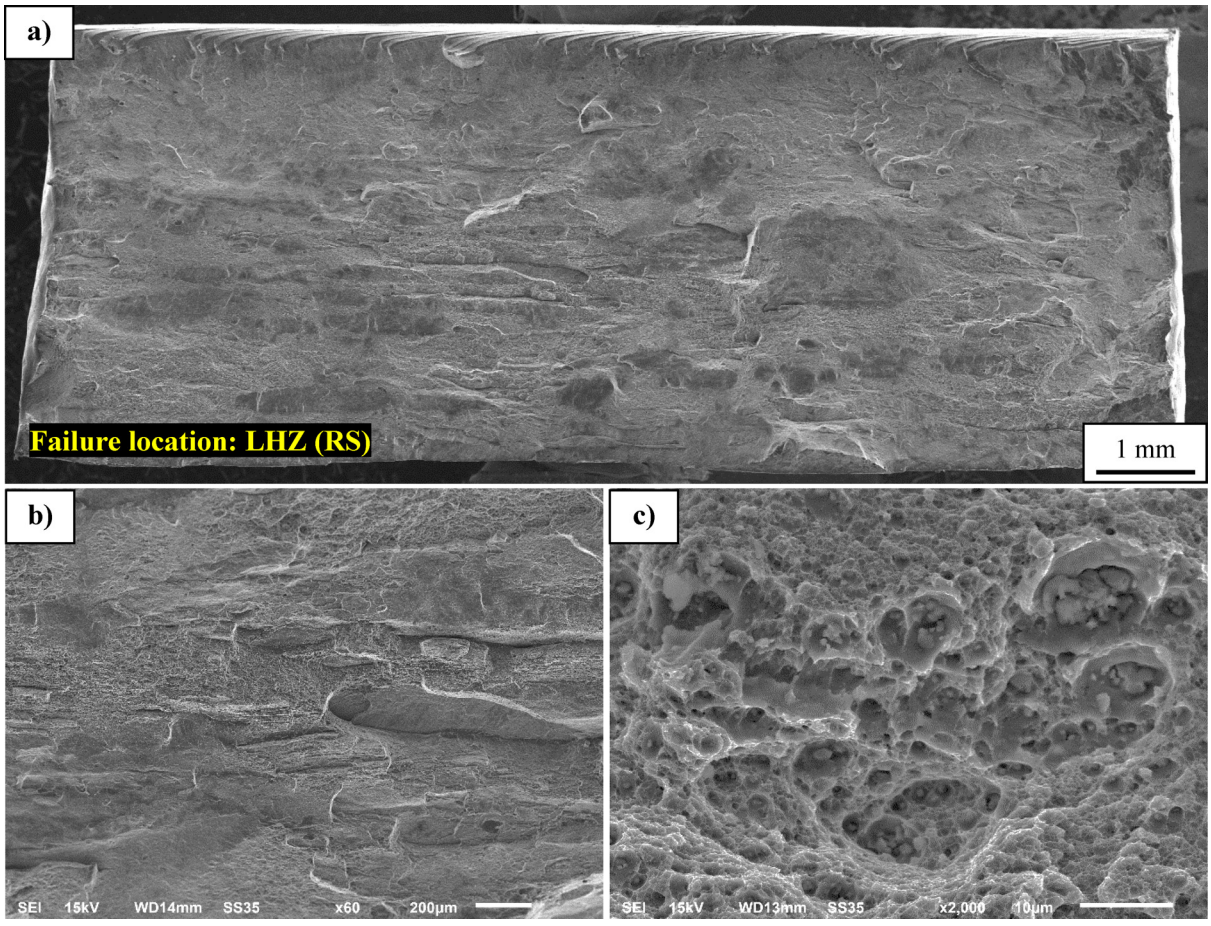

Fig. 8. Fracture surface of FSW joint subjected to tensile test: (a) overall view, (b) local intergranular fracture, (c) dimple structure.

from the base materials value. Analyzing the established values of yield strength (259.9 ± 8.1 MPa) it is possible to observe that the reduction from the base material value (312 MPa) is almost proportional to the drop in ultimate tensile strength. All FSW samples failed in the low hardness zone on the retreating side of the joint, which has been a subject of fracture surface observation using SEM (Figs. 8a–8c).

The surface of the fracture (Fig. 8a) is quite homogenous without significant surface irregularities. This is because the FSW sample has ruptured out of the joint in the heat-affected zone. Figure 8b shows that material has cracked simultaneously in several parallel planes and the individual cracks are combined together by perpendicular interplanar cracks. This character of the fracture results from the texture of the material arising from the production process. Cracking has proceeded in a ductile nature, as evidenced by Figure 8c. Nevertheless, there are present numerous brittle precipitations around which local voids were developed.

The results of low-cycle fatigue testing in the form of the number of cycle vs stress and plastic strain amplitude graphs have been presented below (Figs. 9a,9b).

The analysis of the obtained relationships allows to state that at the total strain amplitude of $\varepsilon_{ac} = 0.3\%$, the investigated joint is characterized by an average value of stress amplitude about $\sigma_a = 215$–225 MPa (Fig. 9a) and the number of cycles to failure within the range of $N_f = 11\,000$–$15\,000$. The friction stir welded joints of AA2519-T62 have three stages of fatigue life: a relatively long period of cyclic hardening (up to 500–1000 cycles), the longest period of cyclic stabilization, and finally the cyclic softening until rapid failure. The number of cycles to failure is correlated with the value of stress amplitude, the greater the stress the lower is sample's fatigue life. At the same time, it can be stated that the plastic strain amplitude contains within the range of $\varepsilon_{ap} = 0.0035$–$0.006\%$ (Fig. 9b). Comparing the low cycle fatigue behavior of the tested joint to the base material, it can be observed that the cyclic hardening period of the FSW joint is far longer and the joint itself is more susceptible to plastic deformation [27,29]. Similar to the tensile samples, the LCF ones also failed in the low hardness zone on the retreating side. The fatigue fracture surface of a representative sample is presented in Figures 10a–10e.

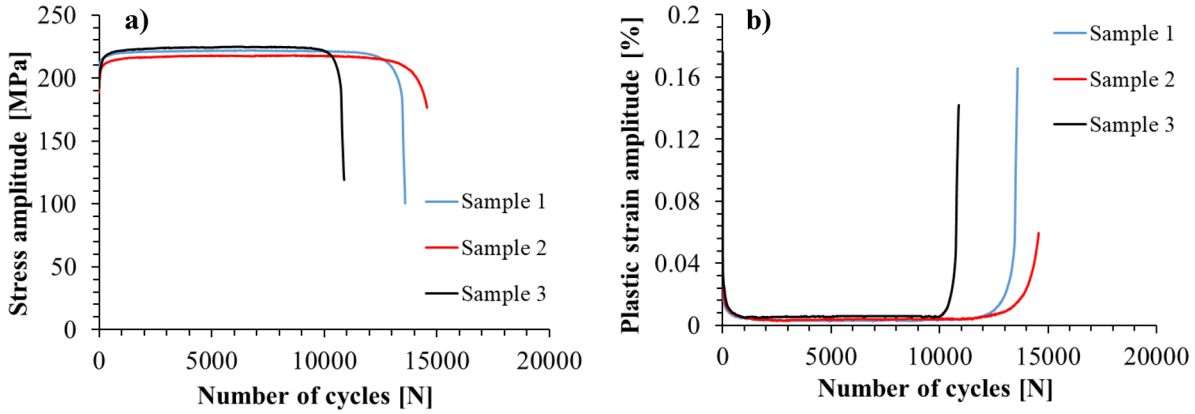

Fig. 9. Number of cycles vs (a) stress amplitude, (b) plastic strain amplitude for the FSW joint.

Observation of the fracture surface has shown that there can be selected two distinct zones, namely a fatigue zone FZ (enveloped in Fig. 10a) and a final rupture zone FR. The cracks have initiated in FZ and then they have propagated steadily as semi-elliptical cracks, what is commonly observed [30–32]. The crack has reached a critical size and the character of propagation has changed at the transition zone, indicated in Figure 10a by the dashed line. The crack growth rate significantly increased until a final rupture occurred. An exemplary crack origin was shown in Figure 10b. Two stages of crack initiation can be recognized. The surface layer with a thickness of ~0.3 mm cracked firstly. The structure in this layer is characterized by overgrowth grains, (see Fig. 4) and probably the crack has in a short time propagated to the transition layer (dashed line), where the fine-grained structure begins to appear. This change of structure caused the propagation to be temporarily stopped. Fatigue lines, typical for the initiation stage, are visible exactly from this layer (the crack growth direction is shown by arrows). Thus, this interlayer can be considered the initial point of fatigue fracture. Although the presence of geometrical irregularities on the weld's face is a potential crack initiator, the fine-grained microstructure beneath it inhibits crack growth. Also, during the fatigue samples preparation, the irregularities have been slightly grounded to minimalize their impact on the fatigue performance. It is a technological operation widely used in the post-processing of FSW joints, and in this case, it allows to obtain a more consistent picture of the influence of microstructure on the fatigue crack initiation and propagation by eliminating geometric notches.

The crack surface of tested samples is irregular, no evident cracks in the crystallographic planes were observed and the cracks propagated rather at the grain boundary or through the grains as a result of developing fatigue cracking (Fig 10c). The evidence confirming the ductile nature of cracking is the fatigue striations shown in Figure 10d. Moreover, the secondary cracks were observed in the zone of high crack growth (Fig. 10e). All presented photos indicate that the decohesion of the investigated alloy is ductile.

The basic, identified factor causing the fatigue crack initiation is the near-surface layer of overgrown grains in the base material, approx. 0.5 mm thick. Such a layer is often formed during the heat treatment of aluminum extrusion and is described in the literature [33]. Although it is not a factor directly related to the FSW process, the joining operation has its impact on it. The layer is completely fragmented in the upper part of the FSW joint due to the affection of the tool shoulder, and in the lower part on the retreating side it is only partially deformed, maintaining its coarse-grained structure (Fig. 4). For this reason, the fatigue crack initiation takes place outside the stirred region, in the places where large grains occur and are additionally weakened by the heat of the welding process, resulting in a partial overaging of the strengthening phase [4,19]. With the development of the crack and its deeper propagation into the material, the weakest link in the FSW connection – the low hardness zone – plays a decisive role [23,34]. It is through this zone, which is located on the border TMAZ/HAZ, a gradual loss of integrity occurs. The low-hardness zone has a width of approx. 2 mm and begins approx. 8 mm from the center of the weld. It should be noted that its microhardness is relatively high (107–113 HV0.1) and significantly differs from other literature reports, mostly around 85 HV0.1 [6,23–24]. The reasons for this should be seen in the use of a relatively low value of tool rotational speed (400 rpm), which significantly reduces the amount of heat affecting the welded material [1,18]. The dominant phenomenon in the formation of the low hardness zone is the overaging of the strengthening phase [23]. The reduction in participation of θ' phase, which is an obstacle to the dislocation movement, facilitates plastic deformation in this area and thus contributes to the ductile character of cracking [1,19,23].

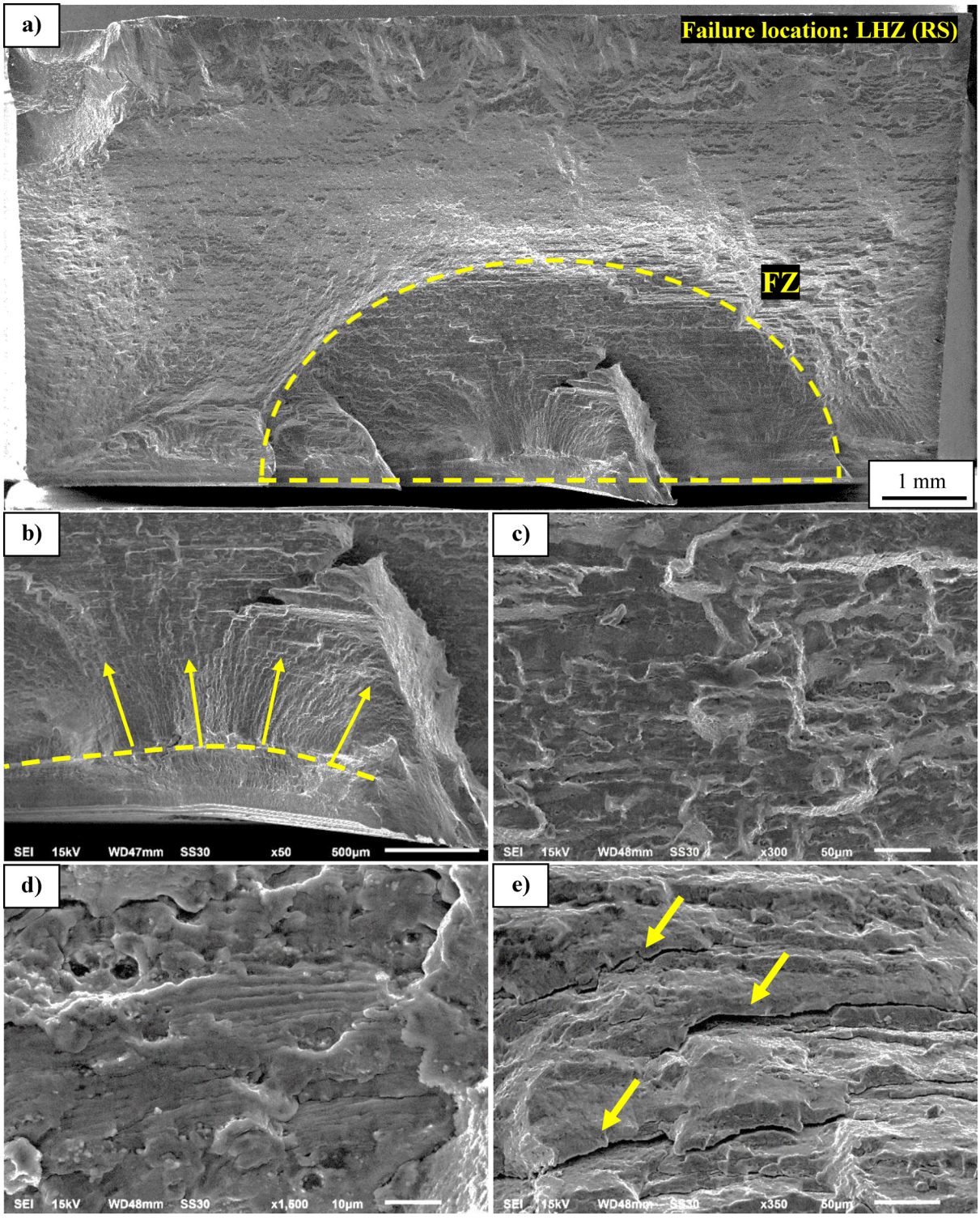

Fig. 10. Fracture surface of the FSW joint subjected to LCF test: (a) overall view, (b) crack initiation site, (c) intergranular fracture, (d) fatigue striation patterns, (e) secondary cracks (marked with yellow arrows).

4 Conclusions

The performed investigation allowed the following conclusions to be drawn:

- The joint's macrostructure does not exhibit any signs of imperfections. On the retreating side, the layer of overgrowth grains undergoes deformation in the TMAZ and forms a specific large-grain band partly surrounding the SZ. The reflection of this phenomenon can be seen in the microhardness distribution at the bottom part of the joint.
- The reported UTS is very high and it equals 405 MPa, what corresponds to 86.5% joint efficiency value. The failure occurred in the LHZ at the retreating side with a fracture mechanism characterized by simultaneously cracking in several parallel planes.
- The LCF behavior of the tested joint indicates three stages of fatigue life: a relatively long period of cyclic hardening (up to 500–1000 cycles), the longest period of cyclic stabilization, followed by the cyclic softening until failure. The fracture surface of tested samples is irregular, no evident cracks in the crystallographic planes were observed and the cracks propagated rather at the grain boundary or through the grains as a result of developing fatigue cracking.
- The fatigue crack initiation takes place in the near-surface layer of overgrown grains and then propagates through the low-hardness zone. The character of fracture is ductile.

Funding

This research was funded by Polish Ministry of National Defence, grant number: PBG/13-998.

References

1. R.S. Mishra, M.W. Mahoney, Friction Stir Welding and Processing, ASM International: Materials Park, OH, USA (2007)
2. A. Siddiquee, A.N. Siddiquee, Z.A. Khan, M. Ubaid, D. Bajaj, M. Atif, A. Khan, Microstructure evolution of friction stir welded dissimilar aerospace aluminium alloys, IOP Conf. Series: Mater. Sci. Eng. **404** (2018) 012002
3. Z.Y. Ma, A.H. Feng, D.L. Chen, J. Shen, Recent advances in friction stir welding/processing of aluminium alloys: microstructural evolution and mechanical properties, Crit. Rev. Solid State Mater. Sci. **43** (2018) 269–333
4. G. Çam, S. Mistikoglu, Recent developments in friction stir welding of Al-alloys, J. Mater. Eng. Perform. **23** (2014) 1936–1953
5. S. Lin, J. Tang, S. Liu, Y. Deng, H. Lin, H. Ji, L. Ye, X. Zhang, Effect of travel speed on microstructure and mechanical properties of FSW joints for Al-Zn-Mg alloy, Materials **12** (2019) 4178
6. S.S. Sabari, S. Malarvizhi, V. Balasubramanian, Characteristics of FSW and UWFSW joints of AA2519-T87 aluminium alloy: effect of tool rotation speed, J. Manuf. Process. **22** (2016) 278–289
7. M. Ubaid, D. Bajaj, A.K. Mukhopadhyay, A.N. Siddiquee, Friction stir welding of thick AA2519 alloy: Defect elimination, mechanical and micro-structural characterization, Met. Mater. Int. (2019) 1–20
8. X.P. Liang, H.Z. Li, Z. Li, T. Hong, B. Ma, S.D. Liu, Y. Liu, Study on the microstructure in a friction stir welded 2519-T87 Al alloy, Mater. Des. **35** (2012) 603–608
9. J. Torzewski, K. Grzelak, M. Wachowski, R. Kosturek, Microstructure and low cycle fatigue properties of AA5083 H111 friction stir welded joint, Materials **13** (2020) 2381
10. J.J. Jr, L.S. Kramer, J.R. Pickens, Aluminum alloy 2519 in military vehicles, Adv. Mater. Process. **160** (2002) 43–46
11. G. Owolabi, T. Daramola, N. Yilmaz, H. Whitworth, A. Zeytinchi, Mechanical properties of ultrafine grain 2519 aluminum alloy, in *TMS Annual Meeting & Exhibition, Proceedings of the 147th Annual Meeting & Exhibition Supplemental TMS, 11–15. 03, Phoenix, Arizona, 11–15 March 2018; The Minerals, Metals & Materials Series*, Springer International Publishing: Cham, Switzerland (2018) pp. 943–950
12. B. Płonka, M. Rajda, Z. Zamkotowicz, J. Zelechowski, K. Remsak, P. Korczak, W. Szymański, L. Sniezek, Studies of the AA2519 alloy hot rolling process and cladding with EN AW-1050A alloy, Arch. Metall. Mater. **61** (2016) 381–388
13. V.V. Zakharov, Combined alloying of aluminium alloys with scandium and zirconium, Met. Sci. Heat Treat. **56** (2014) 281–286
14. Z.H. Jia, J. Røyset, J.K. Solberg, Q. Liu, Formation of precipitates and recrystallization resistance in Al-Sc-Zr alloys, Trans. Nonferrous Met. Soc. China **22** (2012) 1866–1871
15. Y. Chen, J. Feng, H. Liu, Precipitate evolution in friction stir welding of 2219-T6 aluminum alloys, Mater. Charact. **60** (2009) 476–481
16. A. Akram, H. Abdulkadhum, Optimization of friction stir welding process parameters to joint 7075-T6 aluminium alloy by utilizing Taguchi technique, J. Eng. **25** (2019) 1–15
17. R. Kosturek, L. Śnieżek, J. Torzewski, M. Wachowski, The influence of welding parameters on macrostructure and mechanical properties of Sc-modified AA2519-T62 FSW joints, Manuf. Rev. **7** (2020) 28
18. M. Milčić, D. Milčić, T. Vuherer, L. Radovic, I. Radisavljević, A. Djuric, Influence of welding speed on fracture toughness of friction stir welded AA2024-T351 joints, Materials **14** (2021) 1561
19. W. Xu, J.H. Liu, D.L. Chen, G.H. Luan, Low-cycle fatigue of a friction stir welded 2219-T62 aluminum alloy at different welding parameters and cooling conditions, Int. J. Adv. Manuf. Technol. **74** (2014) 209–218
20. O. Hatamleh, The effects of laser peening and shot peening on mechanical properties in friction stir welded 7075-T7351 aluminum, J. Mater. Eng. Perform. **17** (2018) 688–694
21. L. Nie, Y. Wu, G. Hai, D. Chen, X. Guo, Effect of shot peening on redistribution of residual stress field in friction stir welding of 2219 aluminum alloy, Materials **13** (2020) 3169
22. R. Kosturek, L. Sniezek, M. Wachowski, J. Torzewski, The influence of post-weld heat treatment on the microstructure and fatigue properties of Sc-modified AA2519 friction stir-welded joint, Materials **12** (2019) 583
23. Z. Zhang, B. Xiao, Z.Y. Ma, Effect of welding parameters on microstructure and mechanical properties of friction stir welded 2219Al-T6 joints, J. Mater. Sci. **47** (2012) 4075–4086

24. D.G. Mohan, J. Tomków, S. Gopi, Induction assisted hybrid friction stir welding of dissimilar materials AA5052 aluminium alloy and X12Cr13 stainless steel, Adv. Mater. **21** (2021) 17–30
25. G.Q. Sun, J.P. Niu, Y.J. Chen et al., Experimental research on fatigue failure for 2219-T6 aluminum alloy friction stir-welded joints, J. Mater. Eng. Perform. **26** (2017) 3767–3774
26. M. Pitchandi, A. Prabhu, S. Manwatkar, S. Rao, N. Svs, D. Sivakumar, B. Pant, M. Mohan, Tensile and fracture properties of aluminium alloy AA2219-T87 friction stir weld joints for aerospace applications, Metall. Mater. Trans. A **52** (2021) 3759–3776
27. R. Kosturek, L. Śnieżek, J. Torzewski, T. Ślęzak, M. Wachowski, I. Szachogłuchowicz, Research on the properties and low cycle fatigue of Sc-modified AA2519-T62 FSW joint, Materials **13** (2020) 5226
28. W. Wang, P. Han, K. Qiao, T. Li, K. Wang, J. Cai, L. Wang, Effect of the rotation rate on the low-cycle fatigue behavior of friction-stir welded AZ31 magnesium alloy, Eng. Fract. Mech. **228** (2020) 106925
29. R. Kosturek, L. Sniezek, J. Torzewski, M. Wachowski, Low cycle fatigue properties of Sc-modified AA2519-T62 extrusion, Materials **13** (2020) 220–231
30. P.S. Song, B.C. Sheu, Y.L. Shieh, Prediction of semi-elliptical surface crack growth in 2024-T4 aluminium alloy, Int. J. Pres. Ves. Pip. **79** (2002) 273–278
31. L. Śnieżek, T. Ślęzak, K. Grzelak, V. Hutsaylyuk, An experimental investigation of propagation the semi-elliptical surface cracks in an austenitic steel, Int. J. Pres. Ves. Pip. **144** (2016) 35–44
32. J.Y. Xiao, G.Z. Wang, S.T. Tu, F.Z. Xuan, Engineering estimation method of unified constraint parameters for semi-elliptical surface cracks in plates, Eng. Fract. Mech. **229** (2020) 106935
33. W.H. Van Geertruyden, W.Z. Misiolek, P.T. Wang, Surface grain structure development during indirect extrusion of 6xxx aluminum alloys, J. Mater. Sci. **40** (2005) 3861–3863
34. Y. Tao, Z. Zhang, B.H. Yu, P. Xue, D.R. Ni, B.L. Xiao, Z.Y. Ma, Friction stir welding of 2060-T8 AlLi alloy. Part I: Microstructure evolution mechanism and mechanical properties, Mater. Charact. **168** (2020) 110524

Cite this article as: Robert Kosturek, Tomasz Ślęzak, Janusz Torzewski, Marcin Wachowski, Lucjan Śnieżek, Study on tensile and fatigue failure in the low-hardness zone of AA2519-T62 FSW joint, Manufacturing Rev. **9**, 25 (2022)